JAIST Repository
https://dspace.jaist.ac.jp/

Title	Defect termination on crystalline silicon surfaces by hydrogen for improvement in the passivation quality of catalytic chemical vapor-deposited SiN_x and SiN_x/P catalytic-doped layers
Author(s)	Thi, Trinh Cham; Koyama, Koichi; Ohdaira, Keisuke; Matsumura, Hideki
Citation	Japanese Journal of Applied Physics, 55(2S): 02BF09-1-02BF09-6
Issue Date	2016-01-22
Type	Journal Article
Text version	author
URL	http://hdl.handle.net/10119/13833
Rights	This is the author's version of the work. It is posted here by permission of The Japan Society of Applied Physics. Copyright (C) 2016 The Japan Society of Applied Physics. Trinh Cham Thi, Koichi Koyama, Keisuke Ohdaira, and Hideki Matsumura, Japanese Journal of Applied Physics, 55(2S), 2016, 02BF09-1-02BF09-6. http://dx.doi.org/10.7567/JJAP.55.02BF09
Description	

JAIST
JAPAN
ADVANCED INSTITUTE OF
SCIENCE AND TECHNOLOGY

Japan Advanced Institute of Science and Technology

Defect termination on crystalline silicon surfaces by hydrogen for improvement in the passivation quality of catalytic chemical vapor-deposited SiN_x and SiN_x/P catalytic-doped layers

Trinh Cham Thi[1,2,†], Koichi Koyama[1,2], Keisuke Ohdaira[1,2,*], and Hideki Matsumura[1,2]

[1]Japan Advanced Institute of Science and Technology (JAIST),

Nomi, Ishikawa 923-1292, Japan

[2]CREST, Japan Science and Technology Agency (JST),

Kawaguchi, Saitama 332-0012, Japan

E-mail: ohdaira@jaist.ac.jp

We investigate the role of hydrogen (H) in the improvement in the passivation quality of silicon nitride (SiN_x) prepared by catalytic chemical vapor deposition (Cat-CVD) and Cat-CVD SiN_x/phosphorus (P) Cat-doped layers on crystalline silicon (c-Si) by annealing. Both structures show promising passivation capabilities for c-Si with extremely low surface recombination velocity (SRV) on n-type c-Si. Defect termination by H is evaluated on the basis of defect density (N_d) determined by electron spin resonance (ESR) spectroscopy and interface state density (D_{it}) calculated by the Terman method. The two parameters are found to be drastically decreased by annealing after SiN_x deposition. The calculated average D_{it} at midgap ($D_{it\text{-}average}$) is 2.2×10^{11} $eV^{-1}cm^{-2}$ for the SiN_x/P Cat-doped c-Si sample with a SRV of 2 cm/s, which is equivalent to

3.1×10^{11} $eV^{-1}cm^{-2}$ for the SiN_x/c-Si sample with a SRV of 5 cm/s after annealing. The results indicate that H atoms play a critical role in the reduction in D_{it} for SiN_x/c-Si and SiN_x/P Cat-doped c-Si, resulting in a drastic reduction in SRV by annealing.

†Present address: Graduate School of Engineering, Nagoya University, Nagoya 464-8603, Japan

1. Introduction

Passivation layers for crystalline silicon (c-Si) have recently been the focus of much attention owing to their important contribution to the improvement in c-Si solar cell efficiency by the reduction in electrical loss caused by defects at the c-Si surface. Besides high passivation quality, passivation films with high transparency and antireflective properties are more preferable. Silicon nitride (SiN_x), amorphous silicon (a-Si), Al_2O_3, SiO_2, and their stacked layers are excellent passivation layers that demonstrate outstanding passivation quality [1-7]. The passivation of these layers relies on defect termination and/or field-effect passivation. Regarding the defect termination mechanism, the surface recombination of minority carriers is suppressed by the reduction in interface state density (D_{it}), whereas minority carrier recombination probability is decreased by band bending in field-effect passivation. It has been reported that Al_2O_3 films prepared by atomic layer deposition show low surface recombination velocities (SRVs) of 2 and 6 cm/s on 1.9 Ωcm floating zone (FZ) n-type c-Si and 1.5 Ωcm FZ p-type c-Si, respectively [4]. However, Al_2O_3 films do not exhibit antireflective properties on c-Si owing to the mismatch of refractive index. SiO_2 has high passivation quality, and a low SRV of 2.4 cm/s can be obtained for c-Si passivated with SiO_2 films formed by thermal oxidation [3]. However, thermal oxidation requires a high temperature (>1000 ^{o}C), which is not suitable particularly for the fabrication of silicon heterojunction solar cells containing a-Si films with low thermal tolerance. Among these passivation layers, stoichiometric SiN_x films with a refractive index of ~2 is the most promising passivation layer because they show not only excellent passivation quality and high transparency but also significant antireflective properties on c-Si. Moreover, the preparation of SiN_x films does not require a high temperature. A

conventional method used to fabricate SiN_x films is plasma-enhanced chemical vapor deposition (PECVD). PECVD SiN_x films with high passivation quality having SRVs of 2-10 cm/s have been reported [4,5,7]. The passivation mechanism of PECVD SiN_x layers is mainly based on field-effect passivation originating from positive fixed charges in the SiN_x films, whereas thermally grown SiO_2 layers can significantly reduce D_{it}. Typical values of D_{it} and fixed charge density (Q_f) are ~10^{10} $eV^{-1}cm^{-2}$ and ~10^{10} cm^{-2} for SiO_2 and ~10^{11} $eV^{-1}cm^{-2}$ and ~10^{11} cm^{-2} for PECVD SiN_x layers, respectively [8]. Ion bombardment during PECVD tends to deteriorate film/interface quality, and if this problem can be solved, SiN_x films with higher passivation quality will be realized.

Catalytic CVD (Cat-CVD), often also referred to as hot-wire CVD, is one of the potential methods to overcome the drawback of PECVD [9,10]. Radical species are formed by the decomposition of source gas molecules on a heated catalyzing wire in Cat-CVD. c-Si surfaces are thus not exposed to energetic ions, and good film/c-Si interface properties can be realized. Moreover, the H content of Cat-CVD films is lower than that of PECVD films, resulting in higher stability against light exposure [10]. The Cat-CVD system can also be utilized to form ultrathin doping layers by exposing c-Si surfaces to radicals formed by the decomposition of PH_3 or B_2H_6 radicals [11-15]. This doping technique, catalytic doping (Cat-doping), can be applied to the improvement in passivation quality since the thin doping layers formed act as field-effect passivation layers. Single Cat-CVD SiN_x and Cat-CVD SiN_x/phosphorus (P) Cat-doped layer structures can be promising candidates as passivation layers for c-Si. In our previous studies, extremely low SRV_{max} values of 5 and 2 cm/s have been demonstrated for n-type c-Si passivated with Cat-CVD SiN_x and Cat-CVD SiN_x/P Cat-doped layer structures, respectively [13,16]. The SiN_x films used in this study have been confirmed

to have high transparency and good antireflective properties [16]. It should be emphasized that these extremely low SRV_{max} values can be obtained only after postannealing at an appropriate temperature [13,16]. For a Cat-CVD SiN_x/c-Si sample, the significant reduction in SRV by postannealing is supposed to be due to defect termination by hydrogen atoms. For a sample with a P Cat-doped layer, the drastic reduction in SRV is probably due to field-effect passivation induced by P donors and defect termination by H during annealing.

In this study, to quantitatively clarify the role of H in the defect termination effect on the passivation of c-Si surfaces, we focus on the following topics: the etching effect of H atoms on c-Si surfaces during the deposition process, H distribution in the films, defect density (N_d) in SiN_x films, and D_{it} at Cat-CVD SiN_x/c-Si and SiN_x/P Cat-doped c-Si interfaces. The results show that N_d and D_{it} at midgap ($D_{it\text{-}average}$) decrease significantly after annealing. $D_{it\text{-}average}$ drastically decreases from 2×10^{12} to 3×10^{11} $eV^{-1}cm^{-2}$ after annealing. For a sample with a P Cat-doped layer, $D_{it\text{-}average}$ also effectively decreases from 2×10^{12} to 2×10^{11} $eV^{-1}cm^{-2}$ after annealing. The results obtained indicate that H atoms terminate dangling bonds at film/c-Si interfaces. The slightly smaller $D_{it\text{-}average}$ for the sample with a P Cat-doped layer may be the contribution of H atoms in a P Cat-doped layer.

2. Experimental procedure

To clarify the effect of H on the passivation mechanism, we firstly examined the effect of etching by H atoms on c-Si surfaces during SiN_x deposition. A 290-μm-thick n-type (100) FZ Si wafer with a resistivity of 2.5 Ωcm was cleaned in 5% hydrofluoric acid (HF) diluted with deionized (DI) water for 10 s to remove native oxides. The

sample was then passivated with SiN_x films deposited by Cat-CVD under conditions shown in Table I. After that, the SiN_x films were removed in 30% HF diluted with DI water for 5 s. The complete removal of the SiN_x films was confirmed using the Cauchy model of a spectroscopic ellipsometer (J. A. Woollam WVASE32) for data analysis [17]. Surface morphology was then observed by atomic force microscopy (AFM). The surface morphology of bare c-Si after dipping in 30% HF for 5 s was also measured for comparison. For this measurement, two SiN_x deposition conditions were selected. Under one condition, a SiN_x film was deposited at a substrate temperature (T_s) of 100 ^oC, at which the most significant improvement in the passivation quality of SiN_x by annealing is achieved. Under the other condition, SiN_x films were deposited at a T_s of 300 ^oC, at which the highest effective minority carrier lifetime (τ_{eff}) is obtained for an as-deposited sample. The surface morphology of the samples was observed immediately after dipping in DI water and drying with a N_2 gun. H distribution is one of the important factors considered to investigate the passivation mechanism of H in SiN_x films. In this study, the H profiles in SiN_x films before and after annealing at 350 ^oC for 30 min were measured by secondary ion mass spectrometry (SIMS). We evaluated N_d using five 2.5×20 mm^2 quartz glass substrates with 100-nm-thick SiN_x films for each substrate (500 nm in total) by electron spin resonance (ESR) spectroscopy (JEOL JES-FA100) at room temperature. For τ_{eff} measurement, both surfaces of 290-μm-thick n-type (100) FZ Si wafers with a resistivity of 2.5 Ωcm were passivated with SiN_x layers. We carried out microwave photoconductivity decay (μ-PCD) measurement (KOBELCO LTA-1510EP) using a pulse laser with a wavelength of 904 nm and a photon density of 5×10^{13} cm^{-2}. τ_{eff} is expressed as

$$\frac{1}{\tau_{eff}} = \frac{1}{\tau_{bulk}} + \frac{2S}{W} ,$$

where τ_{bulk}, W, and S represent the minority carrier lifetime in c-Si bulk, wafer thickness, and SRV, respectively. In this study, we calculated the maximum SRV (SRV_{max}) by assuming $\tau_{bulk}=\infty$.

In order to accurately confirm defect termination by H atoms on c-Si surfaces, we calculated D_{it} from the high-frequency experimental capacitance-voltage (C-V) curves obtained from metal-insulator-semiconductor (MIS) structures by the Terman method [18,19]. A cross-sectional schematic view of the MIS structure is shown in Fig. 1. The experimental preparation for the sample structure has been described elsewhere [16]. The deposition conditions of SiN_x films are the same as in Ref. 16 and are summarized in Table I. For a sample with P Cat doping, we used the same condition as that under which we obtained the best SRV after annealing, as reported in Ref. 13. The P Cat doping conditions are summarized in Table II. The samples were annealed three times. The first annealing was conducted after P doping at 400 ^{o}C for 30 min, and the second annealing was conducted after SiN_x film deposition at 350 ^{o}C for 30 min. An Al ohmic contact is formed on the back side of the samples by evaporation and annealing at 400 ^{o}C for 10 min. Finally, the front Al electrode was evaporated. A SiN_x/P Cat-doped layer/c-Si sample for lifetime measurement was also prepared and annealed by the same procedure to confirm high passivation quality. The Terman method is mainly based on the comparison of the shapes of the theoretical C-V curve and experimental high-frequency C-V curve. In this study, a high frequency of 1 MHz was used for C-V measurement. C-V curves were measured using a Keithley 6517A electrometer/high resistance meter and a 6440B component analyzer. The theoretical curve was calculated

using the equations shown in Ref. 18. D_{it} as a function of surface potential is calculated using the following equation [19]:

$$D_{it} = \frac{d\left(V_{g_measured} - V_{g_theoretical}\right)}{d\psi_s}\frac{C_i}{q},$$

where V_g is the applied voltage, C_i is the insulator capacitance, q is the elementary charge, and ψ_s is the surface potential.

3. Results and discussion

3.1. H etching during SiN_x deposition

Cat-CVD is a well-known method, which causes no plasma-induced damage to the substrate surface. However, the substrate surface may be etched by H atoms when it is exposed to a high density of H atoms at a T_s lower than 150 ^{o}C [20]. In our study, the lowest SRV_{max} of 5 cm/s was achieved for c-Si passivated with SiN_x films deposited at a T_s of 100 ^{o}C after annealing. All the samples showed high SRV_{max} values (≥30 cm/s) before annealing [16]. One possible reason is supposed to be H etching during SiN_x deposition. However, since the SiN_x deposition rate of ~30 nm/min at a T_s of 100 ^{o}C is sufficiently high, the rapid coverage of the c-Si surface by SiN_x may suppress the effect of H etching. To obtain experimental evidence for this speculation, we investigated the effect of H etching during SiN_x film deposition by evaluating the surface morphology of c-Si after the deposition and removal of SiN_x films. We firstly deposited SiN_x films on the c-Si surface and then examined the surface morphology of the sample after removing the SiN_x films using HF solution. The thickness and refractive index of the SiN_x films were 80 nm and ~2.0, respectively; however, no such films were observed at

all by spectroscopic ellipsometry after HF dipping. This observation indicates that SiN_x was completely removed from c-Si surfaces.

Figure 2 shows the AFM images of c-Si surfaces after the removal of the SiN_x films. The morphology of the c-Si surface without SiN_x deposition after dipping in HF is also shown for comparison. For the sample without SiN_x film deposition, the root-mean-square roughness (R_{rms}) of the c-Si surface is 0.095 nm, whereas those of the samples with SiN_x deposition at T_s values of 100 and 300 ^oC are 0.13 and 0.10 nm, respectively. The R_{rms} of the bare c-Si surface dipped in HF solution is comparable to those of the samples without HF etching, as reported in Ref. 13. This suggests that the c-Si surface does not deteriorate after dipping in 30% HF for 5 s. The slightly higher R_{rms} values obtained for the samples with SiN_x deposition and removal indicate that etching occurs during SiN_x deposition. The R_{rms} of the sample with a SiN_x film deposited at 300 ^oC is lower than that of the sample with a SiN_x film deposited at 100 ^oC. H etching during SiN_x film deposition might therefore be a possible reason for the higher τ_{eff} of an as-deposited SiN_x/c-Si structure with SiN_x deposited at a higher T_s. However, since a low SRV_{max} of 5 cm/s is obtained for the SiN_x/c-Si structure with SiN_x films deposited at a T_s of 100 ^oC, the effect of etching by atomic hydrogen during SiN_x deposition on passivation quality may be negligible.

3.2. H distributions in SiN_x films before and after annealing

The improvement in the passivation quality of SiN_x films by annealing has been reported by many groups [21-23]. The H distribution in SiN_x films is one of the key factors affecting the termination of defects on c-Si surfaces by H atoms during

annealing. The distribution of H atoms inside SiN_x films can provide information on H diffusion or release to the environment during annealing, which may lead to the profound understanding of the H defect termination mechanism. In our previous report, H content was calculated from Fourier-transform infrared (FT-IR) spectra using the Lanford method [16, 24]. We found that the Si-H bonding peak signal intensity slightly increases after annealing. The integrated intensity of the Si-H bonding peak signal increases by ~10% after annealing, whereas no change in that of the N-H bonding peak signal is observed. This suggests that H atoms terminate the Si dangling bond inside c-Si and also at the SiN_x/c-Si interface during annealing. We also supposed that H atoms diffuse into the SiN_x/c-Si interface, and that more dangling bonds are terminated during annealing [16].

Figure 3 shows the SIMS profiles of H concentration in SiN_x films deposited at a T_s of 100 ^{o}C before and after annealing at 350 ^{o}C for 30 min. The H concentration is constant with the depth of SiN_x films. One can see in Fig. 3 that there is no significant difference in H concentration between the samples before and after annealing. Note that the H concentration calculated from the FT-IR spectra of the samples is based on Si-H and N-H bonds in SiN_x films. The integrated intensity of the Si-H bonding peak signal increases when the SiN_x films are annealed at 350 ^{o}C. The SIMS profiles suggest that not diffusion but bonding rearrangement during annealing contributes to defect termination, resulting in the improvement in passivation quality. A possible mechanism is that H atoms exiting in voids inside SiN_x and at the SiN_x/c-Si interface recombine with neighboring Si dangling bonds. In order to confirm defect termination by annealing, in the next subsection, we will report on N_d in SiN_x films and D_{it} at the SiN_x/c-Si interfaces.

3.3. N_d in SiN_x films and D_{it} at SiN_x/c-Si interfaces

Si dangling bonds back-bonded to three N atoms, $N_3{\equiv}Si\cdot$, generally called K centers, are the main dangling bonds in SiN_x films. A K center has three states: K^0, K^-, and K^+ [25-32]. K^+ is the origin of fixed charges in SiN_x films and is easily determined by the negative shift of C-V curves [29-32]. K^0 is a dangling bond containing an unpaired electron and is observable by ESR spectroscopy [25-28]. We have reported that both K^0, corresponding to N_d, and K^+, corresponding to Q_f, decrease markedly after annealing [16]. In particular, for a SiN_x film deposited at a T_s of 100 ^oC, Q_f decreases from $1{\times}10^{12}$ to $7{\times}10^{11}$ cm^{-2} and N_d decreases from $2{\times}10^{18}$ to $4{\times}10^{17}$ cm^{-3} after annealing. Figure 4 shows the ESR spectra of SiN_x films deposited at various T_s values before and after annealing at 350 ^oC for 30 min. The g values obtained were 2.0033-2.0047 for SiN_x films deposited at various T_s values, and the films deposited at lower T_s values resulted in higher g values. The g reported for the K^0 defects is 2.003 [25], and that for Si dangling bonds in a-Si is 2.0055 [33]. The g value of SiN_x films must thus depend on the chemical composition of the films. The g values obtained in this study may imply that the SiN_x films formed are slightly Si-rich, particularly for those formed at lower T_s values. This is reasonable because the SiN_x films are formed so that their refractive indices become 2 and the films formed at lower T_s values have lower densities. From Fig. 4, one can see that the intensities of dangling bond peak signals decrease greatly after annealing. This is clear evidence of defect termination by H in SiN_x films during annealing. This result implies that H can terminate defects not only inside SiN_x but also

on a SiN_x/c-Si interface during annealing, which can lead to a drastic reduction in SRV_{max} after annealing.

To demonstrate more clearly the effect of defect termination by H atoms at the interface of a SiN_x/c-Si structure, we estimated the D_{it} of these samples from their C-V curves by the Terman method. Figure 5 shows the experimental and theoretical C-V curves of the MIS structures with SiN_x films deposited at a T_s of 100 °C before and after annealing. The theoretical C-V curves are drawn under the assumption of no D_{it}. Because positive fixed charges exist in SiN_x films, the experimental C-V curves were negatively shifted. In the figures, we positively shifted the experimental C-V curves by the flat band voltage values to see clearly the difference between the theoretical and experimental C-V curves. One can see that there is a marked difference in shape between the theoretical and experimental C-V curves of the samples before annealing, whereas a good fitting of the theoretical and experimental curves is obtained for the samples after annealing. This result implies that the samples have higher D_{it} values before annealing than after annealing. According to the results of analysis by the Terman method, the D_{it} values of the samples before annealing are on the order of 10^{12} $eV^{-1}cm^{-2}$, whereas those of the samples after annealing are on the order of 10^{11} $eV^{-1}cm^{-2}$. Figure 6 shows the D_{it} values of SiN_x/c-Si structures as a function of surface potential for SiN_x samples deposited at T_s values of 70 and 100 ^oC before and after annealing. A significant decrease in $D_{it\text{-}average}$ is observed for the samples after annealing. This observation is consistent with the improvement in passivation quality and the resulting reduction in SRV. In particular, in the case of the sample deposited at 100 ^oC, which demonstrates a low SRV_{max} of 5 cm/s after annealing, the experimental and ideal C-V curves show the best coincidence and the $D_{it\text{-}average}$ calculated is 3.1×10^{11} $eV^{-1}cm^{-2}$.

Figure 7 shows the SRV_{max} values of the SiN_x/c-Si samples deposited at various T_s values before and after annealing at 350 ^oC for 30 min as a function of $D_{it\text{-}average}$. For the samples before annealing with large SRV_{max} values, the $D_{it\text{-}average}$ values are on the order of 10^{12} $eV^{-1}cm^{-2}$. $D_{it\text{-}average}$ decreases to the order of 10^{11} $eV^{-1}cm^{-2}$ after annealing, by which a SRV_{max} lower than 10 cm/s can be obtained. We suppose that the SRVs of the samples after annealing are strongly affected by $D_{it_average}$ rather than by Q_f; thus, SRV_{max} increases linearly with $D_{it\text{-}average}$. On the other hand, the samples before annealing have higher Q_f and $D_{it_average}$, and both of the two parameters contribute greatly to the passivation mechanism. The linear tendency of SRV against $D_{it_average}$ could thus not be obtained for the samples before annealing. The drastic decrease in D_{it} after annealing strongly supports the speculation that H atoms terminate defects at a SiN_x/c-Si interface. The calculated result in our study is in good agreement with previous reports on PECVD SiN_x films [8,29,34,35]. Wan *et al.* reported the D_{it} of PECVD SiN_x/c-Si interfaces estimated by the Terman method [34]. From their report, SRV_{max} becomes less than 10 cm/s when D_{it} is on the order of 10^{10} $eV^{-1}cm^{-2}$ and Q_f ~10^{11} cm^{-2}. SRV_{max} >100 cm/s corresponds to D_{it} >10^{12} $eV^{-1}cm^{-2}$ and Q_f ~ 10^{12} cm^{-2}. These are consistent with D_{it} and SRV_{max} obtained in our study. Our Cat-CVD SiN_x films have Q_f >10^{11} cm^{-2} even after annealing. The passivation quality of SiN_x films on c-Si depends on not only D_{it} but also Q_f. A Q_f of 7×10^{11} cm^{-2} and a D_{it} of 3.1×10^{11} $eV^{-1}cm^{-2}$ are typical values for the lowest SRV_{max} obtained for c-Si passivated with Cat-CVD SiN_x films.

3.4. D_{it} at SiN_x/P Cat- doped c-Si interface

As reported previously, P Cat doping contributes significantly to the improvement in the passivation quality of SiN_x/c-Si structures. A significantly low SRV_{max} of 2 cm/s has been achieved for a SiN_x/P Cat-doped c-Si structure after annealing [13]. The drastic reduction in SRV_{max} is supposed to be mainly due to the field effect passivation induced by P donors. The P doping process is conducted at a low T_s of 80 ^{o}C and the sample surface is exposed to a large number of H atoms, and H etching may occur. Etching can increase surface area, generate more dangling bonds, and/or cause insufficient film coverage on the c-Si surface. On the other hand, H inside the P Cat-doped layer may terminate dangling bonds at the interface of SiN_x/P Cat-doped c-Si and contribute to the reduction in SRV during annealing.

Figure 8 shows the D_{it} values of SiN_x/P Cat-doped c-Si and SiN_x/c-Si samples after annealing at 350 ^{o}C for 30 min. The $D_{it\text{-}average}$ of the SiN_x/P Cat-doped c-Si sample is 2.0×10^{12} $eV^{-1}cm^{-2}$ before annealing, whereas it decreases to 2.1×10^{11} $eV^{-1}cm^{-2}$ after annealing. Those values are equivalent to those of the SiN_x/c-Si sample. We can thus assume that H atoms in a SiN_x film contribute greatly to defect termination on a c-Si surface even in the case of samples with P Cat-doped layers. The reason for the slightly smaller D_{it} of the SiN_x/P Cat-doped c-Si sample than that of the SiN_x/c-Si sample might be the effect of H atoms contained in a P Cat-doped layer. Taken together, we can conclude that both field effect passivation and H defect termination contribute significantly to the improvement in the passivation quality of SiN_x/P Cat-doped c-Si structures.

4. Conclusions

H atoms play an important role in the reduction in SRV for both SiN_x/P Cat-doped c-Si and SiN_x/c-Si samples. Although the c-Si surface is damaged slightly by H etching during P Cat doping and film deposition, H atoms inside SiN_x films can terminate a large number of defects at SiN_x/c-Si interfaces during annealing, resulting in the marked improvement in film passivation quality. $D_{it\text{-}average}$ drastically decreases from 2×10^{12} to 3×10^{11} $eV^{-1}cm^{-2}$ after annealing in the SiN_x/c-Si structure. For the sample with a P Cat-doped layer, $D_{it\text{-}average}$ is also effectively reduced from 2×10^{12} to 2×10^{11} $eV^{-1}cm^{-2}$ by annealing. The low $D_{it\text{-}average}$ obtained indicates the good interface quality of Cat-CVD film/c-Si. The results obtained also demonstrate that H atoms play an important role in the improvement in the passivation quality of SiN_x/c-Si and SiN_x/P Cat-doped c-Si structures.

Acknowledgement

We would like to acknowledge the JST CREST program.

References

[1] R. Hezel and K. Jaeger, J. Electrochem. Soc. **136**, 518 (1989).

[2] A. Focsa, A. Slaoui, H. Charifi, J. P. Stocquert, and S. Roques, Mater. Sci. Eng. B **159-160**, 242 (2009).

[3] M. J. Kerr and A. Cuevas, Semicond. Sci. Technol. **17**, 35 (2002).

[4] B. Hoex, J. Schmidt, P. Pohl, M. C. M. van de Sanden, and W. M. M. Kessels, J. Appl. Phys. **104**, 044903 (2008).

[5] J. Schmidt and M. Kerr, Sol. Energy Mater. Sol. Cells **65**, 585 (2001).

[6] Y. Larionova, V. Mertens, N. Harder, and R. Brendel, Appl. Phys. Lett. **96**, 32105 (2010).

[7] S. Duttagupta, B. Hoex, and A. G. Aberle, presented at 22nd Int. Photovoltaic Science and Engineering Conf., 2012.

[8] S. W. Glunz, Adv. OptoElectron. **2007**, 2 (2007).

[9] H. Matsumura, J. Appl. Phys. **65**, 4396 (1989).

[10] R. E. I. Schropp, ECS Trans. **25**, 3 (2009)

[11] H. Matsumura, M. Miyamoto, K. Koyama, and K. Ohdaira, Sol. Energy Mater. Sol. Cells **95**, 797 (2011).

[12] T. Hayakawa, Y. Nakashima, M. Miyamoto, K. Koyama, K. Ohdaira, and H. Matsumura, Jpn. J. Appl. Phys. **50**, 121301 (2011).

[13] T. C. Thi, K. Koyama, K. Ohdaira, and H. Matsumura, J. Appl. Phys. **116**, 114502 (2014).

[14] H. Matsumura, T. Hayakawa, T. Ohta, Y. Nakashima, M. Miyamoto, T. C. Thi, K. Koyama, and K. Ohdaira, J. Appl. Phys. **116**, 044510 (2014).

[15] T. Ohta, K. Koyama, K. Ohdaira, and H. Matsumura, Thin Solid Films **575**, 92

(2015).

[16] T. C. Thi, K. Koyama, K. Ohdaira, and H. Matsumura, Jpn. J. Appl. Phys. **53**, 022301 (2014).

[17] Guide to Using WVASE32^{TM}: Software for Vase and M-44 Ellipsometers (J. A. Woollam, Lincoln, NE, 1989) p. 159.

[18] E. H. Nicollian and J. R. Brews, *MOS Physics and Technology* (Wiley, New York, 1982) 3rd ed., pp. 99 and 325.

[19] D. K. Schroder, *Semiconductor Device and Characterization* (Wiley, New York, 2006) p. 351.

[20] H. Matsumura, K. Kamesaki, A. Masuda, and A. Izumi, Jpn. J. Appl. Phys. **40**, L289 (2001).

[21] B. Sopori, R. Reedy, K. Jones, Y. Yan, and M. Al-Jassim, Proc. 31st IEEE Photovoltaic Specialists Conf., 2005, p. 1039.

[22] J. Hong, W. M. M. Kessels, M. J. Soppe, A. W. Weeber, W. M. Arnoldbik, and M. C. M. Van de Sanden, J. Vac. Sci. Technol. B **21**, 2123 (2003).

[23] V. Yelundur, A. Rohatgi, J. I. Hanoka, and R. Reedy, Proc. 19th European Photovoltaic Solar Energy Conf., 2004, p. 951.

[24] W. A. Lanford, J. Appl. Phys. **49**, 2473 (1978).

[25] D. T. Krick, P. M. Lenahan, and J. Kanicki, J. Appl. Phys. **64**, 3558 (1988).

[26] P. M. Lenahan, D. T. Krick, and J. Kanicki, Appl. Surf. Sci. **39**, 392 (1989).

[27] P. M. Lenahan and S. E. Curry, Appl. Phys. Lett. **56**, 157 (1990).

[28] W. L. Warren and P. M. Lenahan, Phys. Rev. B **42**, 1773 (1990).

[29] J. -F. Lelièvre, E. Fourmond, A. Kaminski, O. Palais, D. Ballutaud, and M. Lemiti, Sol. Energy Mater. Sol. Cells **93**, 1281 (2009).

[30] L. Xiangna, Z. Zhouyin, and W. Yong, Chin. Phys. Lett. **7**, 79 (1990).

[31] J. Robertson, W. L. Warren, and J. Kanicki, J. Non-Cryst. Solids **187**, 297 (1995).

[32] W. L. Warren, J. Robertson, and J. Kanicki, Appl. Phys. Lett. **6**, 2685 (1993).

[33] R. A. Street, *Hydrogenated Amorphous Silicon*, Solid State Science Series, (Cambridge University Press, Cambridge, U.K., 1991) Cambridge Solid State Science Series, p. 107

[34] Y. Wan, K. R. McIntosh, and A. F. Thomson, AIP Adv. **3**, 032113 (2013).

[35] S. Duttagupta, F. Lin, M. Wilson, M. B. Boreland, B. Hoex, and A. G. Aberle, Prog. Photovoltaics **22**, 641 (2012).

Figure captions

Fig.1. Cross-sectional schematic view of a sample used for C-V measurement.

Fig. 2. AFM images of c-Si surfaces after removing SiN_x films. (a) Bare c-Si dipped in 30% HF for 5 s, (b) c-Si after removing a SiN_x film deposited at a T_s of 100 ^oC, and (c) c-Si after removing a SiN_x film deposited at a T_s of 300 ^oC.

Fig. 3. SIMS profiles of H atoms in SiN_x films deposited at a T_s of 100 ^oC before and after annealing at 350 ^oC for 30 min.

Fig. 4. ESR spectra of SiN_x films deposited at various T_s values before and after annealing at 350 ^oC for 30 min.

Fig. 5. Experimental and theoretical C-V curves of the MIS structures with SiN_x films deposited at a T_s value of 100 °C before annealing at 350 ^oC and after annealing for 30 min.

Fig. 6. D_{it} values of SiN_x/c-Si interfaces with SiN_x films deposited at 70 and 100 ^oC before annealing at 350 ^oC and after annealing at 350 ^oC for 30 min as a function of surface potential.

Fig. 7. SRV_{max} values of SiN_x/c-Si samples deposited at various T_s values before and after annealing at 350 ^oC for 30 min as a function of $D_{it\text{-}average}$. Red circles and black square dots represent the values of the samples before and after annealing, respectively.

Fig. 8. D_{it} values of SiN_x/P Cat-doped c-Si and SiN_x/c-Si interfaces after annealing at 350 ^oC for 30 min as a function of surface potential.

Table I. Deposition conditions of SiN_x films.

Film	SiH_4 (sccm)	NH_3 (sccm)	Gas pressure (Pa)	T_s (^oC)	T_{cat} (^oC)	Duration (s)
1	8.7	150	10	50	1800	144
2	8.4	150	10	70	1800	160
3	8	150	10	100	1800	190-210
4	7	150	10	150	1800	220
5	6	150	10	200	1800	240
6	5.3	150	10	300	1800	300

Table II. P Cat doping conditions.

Gas source	He-diluted 2.25% PH_3 20 sccm
Substrate temperature	90 ^oC
Pressure	1 Pa
Catalyzer temperature	1300 ^oC
Exposure duration	60 s

Figure 1.

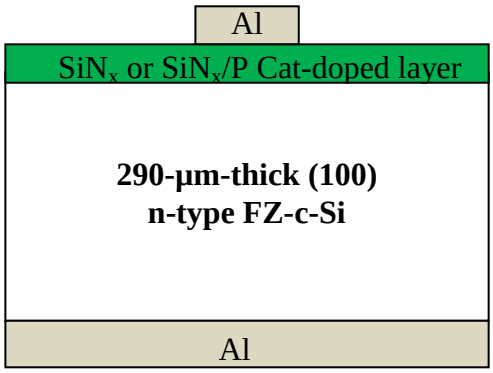
Al
SiNx or SiNx/P Cat-doped layer
290-µm-thick (100)
n-type FZ-c-Si
Al

Figure 2.

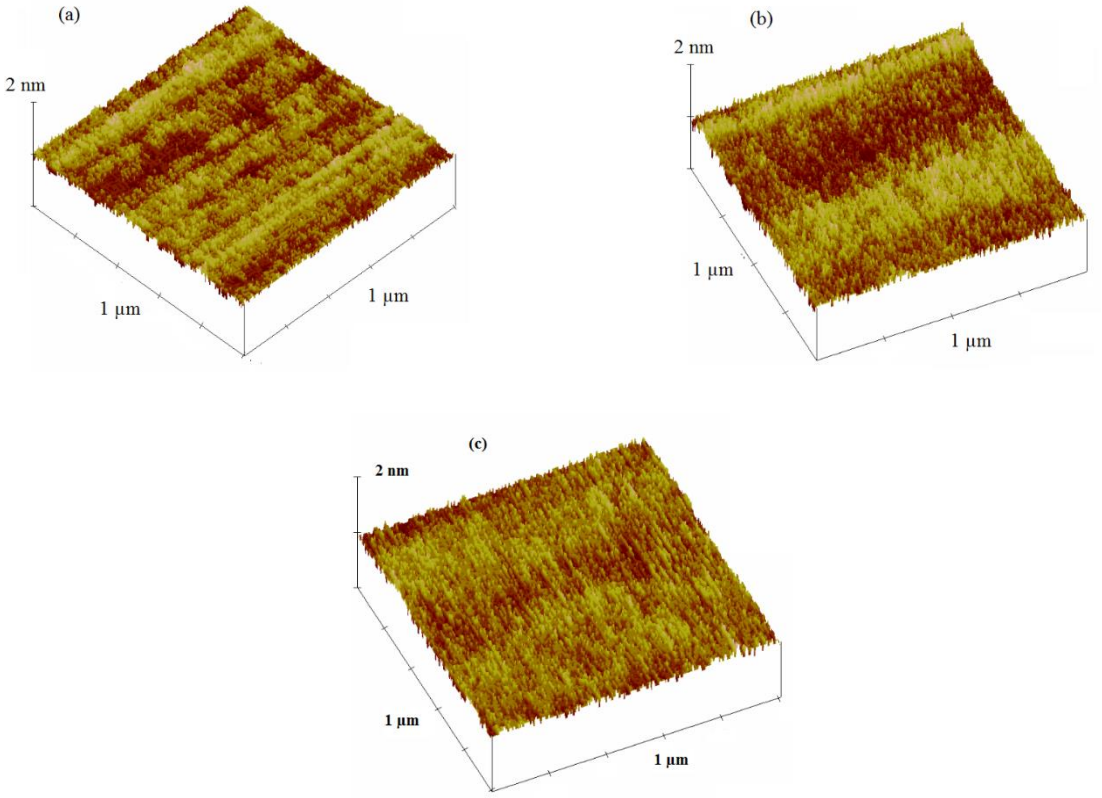

Figure 3

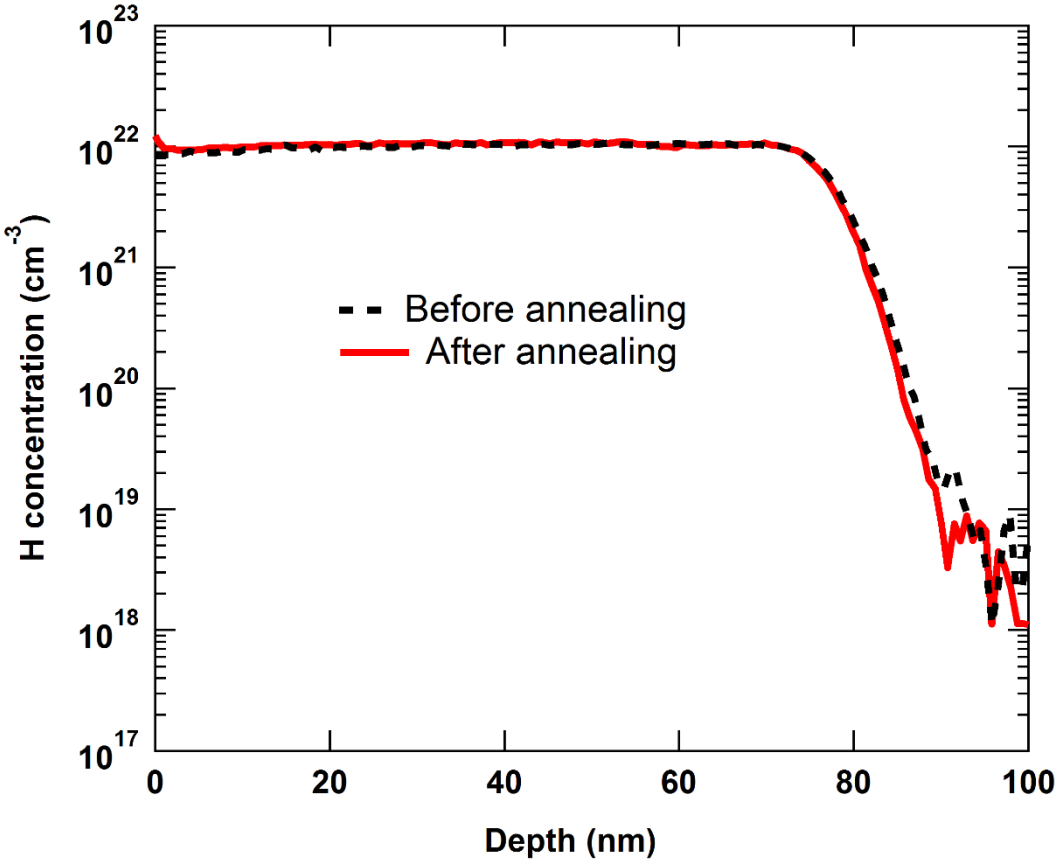
H concentration (cm-3)
10^23
10^22
10^21
10^20
10^19
10^18
10^17
0
20
40
60
80
100
Depth (nm)
Before annealing
After annealing

Figure 4

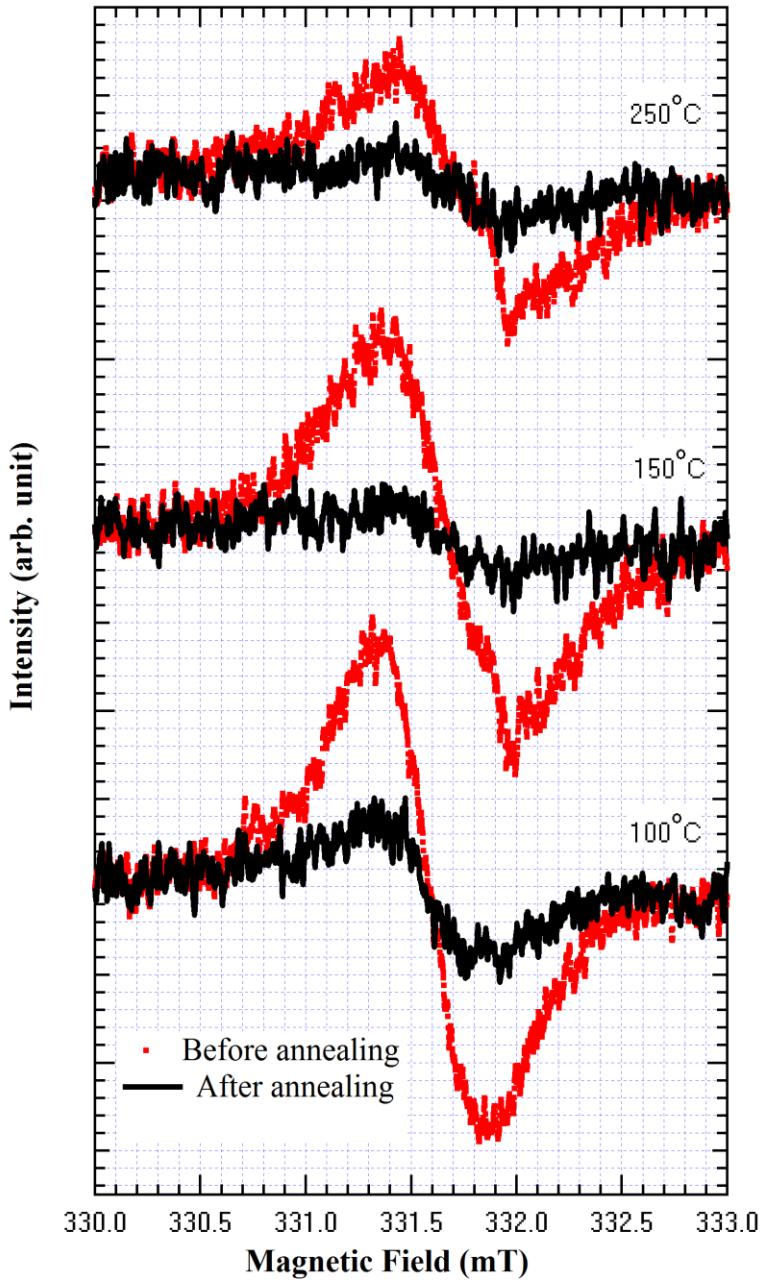
250°C
150°C
100°C
Before annealing
After annealing
Intensity (arb. unit)
330.0
330.5
331.0
331.5
332.0
332.5
333.0
Magnetic Field (mT)

Figure 5

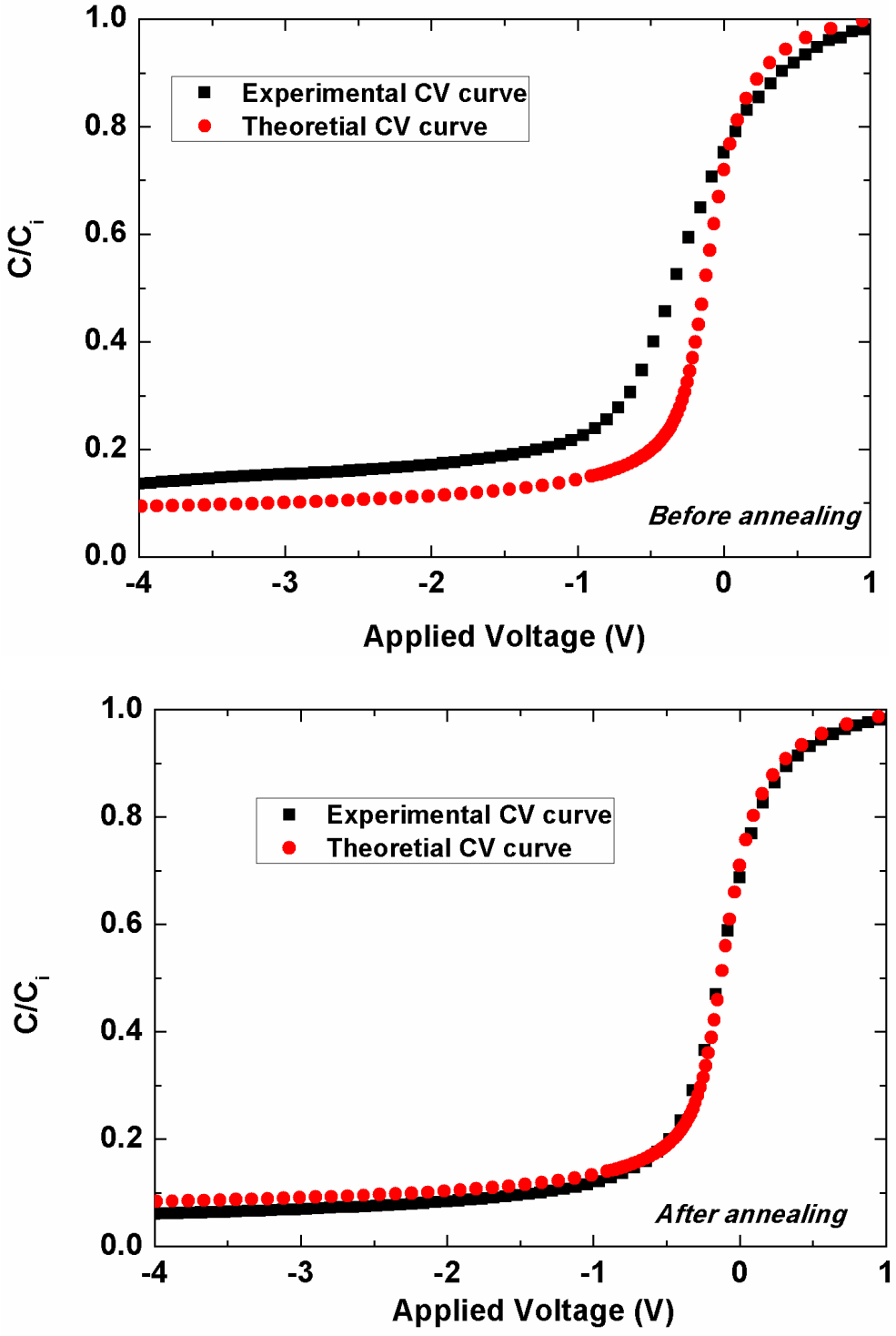
Experimental CV curve
Theoretial CV curve
Before annealing
C/C_i
Applied Voltage (V)
1.0
0.8
0.6
0.4
0.2
0.0
-4
-3
-2
-1
0
1
Experimental CV curve
Theoretial CV curve
After annealing
C/C_i
Applied Voltage (V)

Figure 6

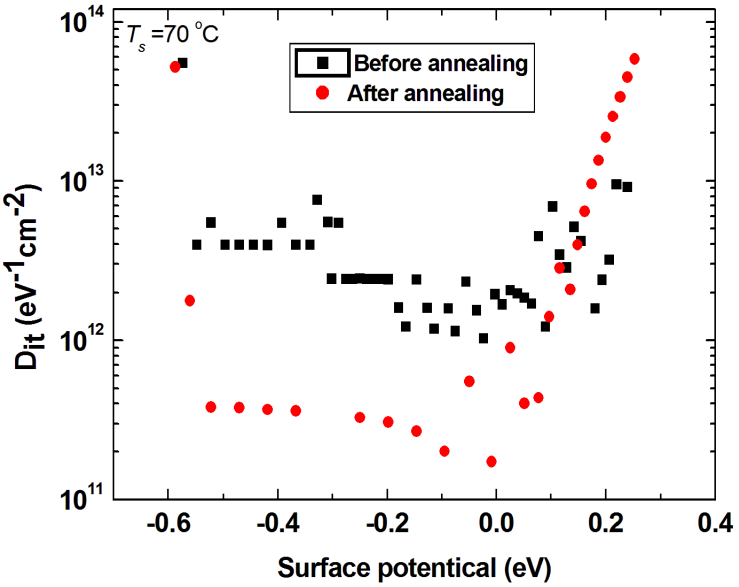
T_s =70 °C
Before annealing
After annealing
D_{it} (eV^{-1}cm^{-2})
10^{14}
10^{13}
10^{12}
10^{11}
-0.6
-0.4
-0.2
0.0
0.2
0.4
Surface potentical (eV)

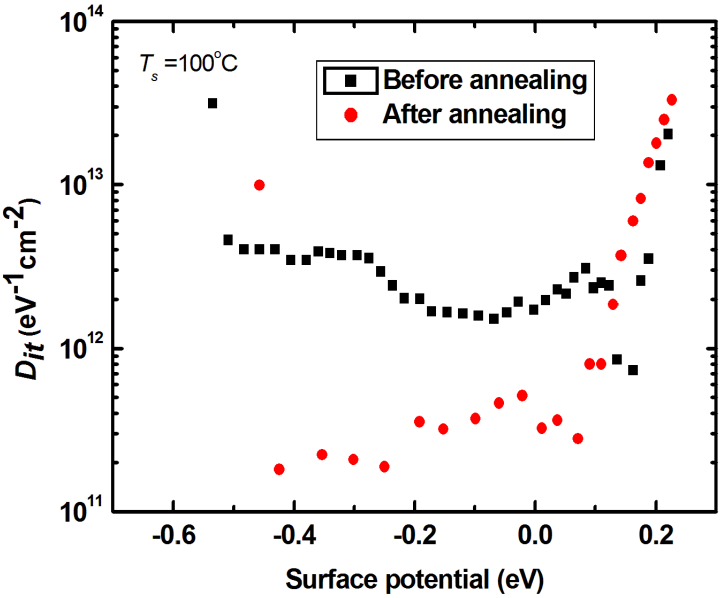
T_s =100°C
Before annealing
After annealing
D_{it} (eV^{-1}cm^{-2})
10^{14}
10^{13}
10^{12}
10^{11}
-0.6
-0.4
-0.2
0.0
0.2
Surface potential (eV)

Figure 7

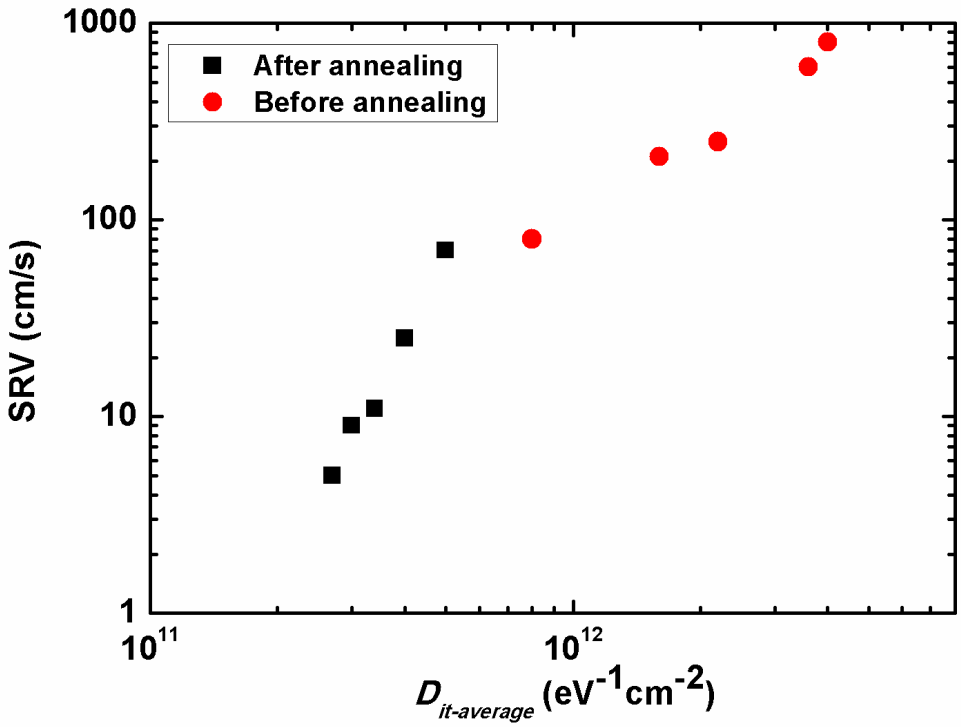
1000
100
10
1
SRV (cm/s)
After annealing
Before annealing
10^11
10^12
D_it-average (eV^-1cm^-2)

Figure 8

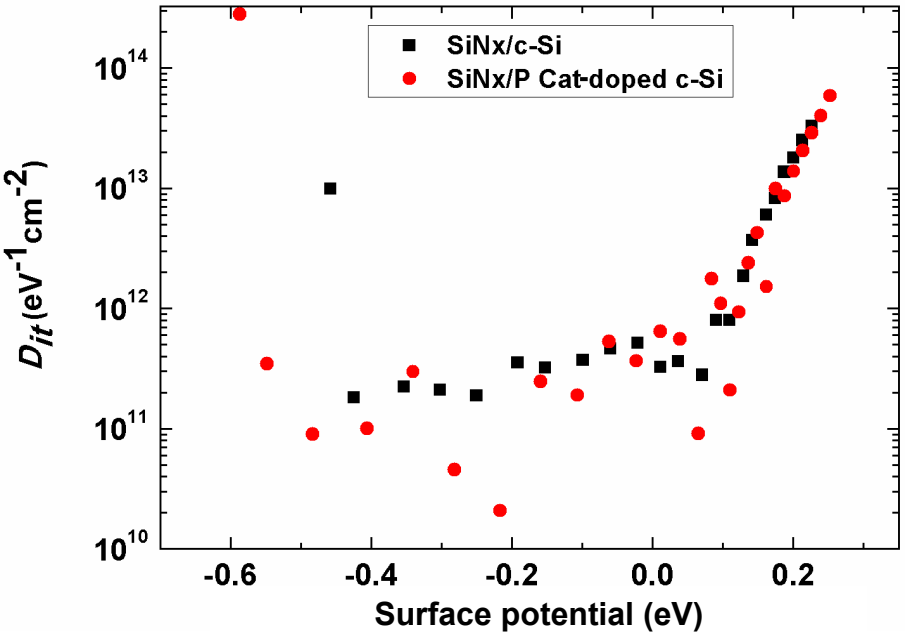
SiNx/c-Si
SiNx/P Cat-doped c-Si
D_{it}(eV^{-1}cm^{-2})
10^{14}
10^{13}
10^{12}
10^{11}
10^{10}
-0.6
-0.4
-0.2
0.0
0.2
Surface potential (eV)